Anisotropic Lennard-Jones fluids in a nanochannel

R.M. Hartkamp and S. Luding

Multiscale Mechanics, Faculty of Engineering Technology, University of Twente, Enschede, 7500AE, The Netherlands

r.m.hartkamp@utwente.nl and s.luding@utwente.nl

Keywords: Molecular dynamics, Lennard-Jones, anisotropy, layering, virial stress

Abstract

During the past few decades molecular dynamics has been a widely applied tool to simulate fluid confined in micro/nano geometries. What makes interfacial fluids fundamentally different from the bulk fluid is the fact that their density varies considerably over microscopic distances. A class of such strongly inhomogeneous fluids are fluids confined in very narrow channels by solid boundaries. In this work, the goal is to study the density and stress terms across the channel.

We simulate planar Poiseuille flow of a Lennard-Jones fluid in channels of various widths in the nanoscale regime. A body force and a local thermostat are applied in order to simulate a steady-state flow. Layering and anisotropy in stress are obtained near the walls of the channel, which leads to non-Newtonian rheology. Understanding and quantifying the non-Newtonian behavior is a first step towards deriving a constitutive model that describes locally the behavior of a strongly confined fluid.

Nomenclature

Roman symbols

b	Bin width
f^*	Reduced body force
F	Interaction force
m	Particle mass
N	Number of particles
p	Hydrostatic pressure
r	Interaction distance
r_c	Cut-off radius
t	Time
T	Period of oscillation
T^*	Reduced temperature
u	Streaming velocity
U	Interaction potential
v	Particle velocity
$\tilde{v}$	Fluctuation velocity
V	Volume
W	Channel width

Greek symbols

ϵ	Energy scale
ϵ_{ij}	Deformation tensor
ν	Volume fraction
Π_{ij}	Stress tensor
ρ^*	Reduced density
σ	Length scale
τ	Natural time step
Φ	Coarse graining function

Miscellaneous

$(\ldots)^p$	Particle property
$(\ldots)^{pq}$	Interaction property
$(\ldots)^k$	Kinetic stress property
$(\ldots)^u$	Potential stress property

Introduction

Molecular dynamics simulations have become an important tool for the study of microscopic fluid properties. A channel geometry is often used to study the inhomogeneous behavior of strongly confined fluids [Koplik & Banavar (1988); Bitsanis *et al.* (1988); Todd & Evans (1995); Travis *et al.* (1997); Travis & Gubbins (2000)]. However, our understanding of these non-Newtonian fluid problems is still very limited, while gaining a deeper insight is becoming increasingly important with the rise of microfluidic and nanofluidic applications, such as lab-on-a-chip devices [van den Berg *et al.* (2009)]. Similar phenomenology (i.e. layering, anisotropy) is observed in many particle systems [van Gunsteren *et al.* (1984); Ghosh *et al.* (2007)]. In this study, liquid argon is confined between two flat walls with a normal in the x-direction (Fig. 1). When an atom leaves the system in y- or z-direction, it re-enters at
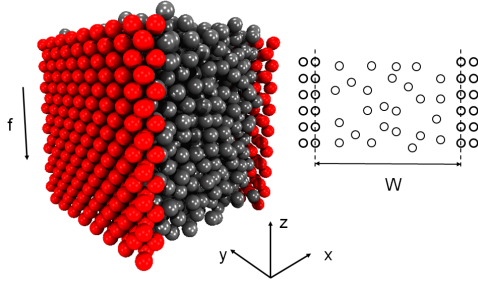
Figure 1: Liquid argon (grey, 1536 atoms) confined between solid argon walls (red, 512 atoms). The width of the channel is defined as shown on the right.

Figure 2: Density profile for three different channels with width $W_1 = 5.985\sigma$ (blue), $W_2 = 11.115\sigma$ (red) and $W_3 = 16.245\sigma$ (black). The vertical lines represent the location of the right wall for that system.

the opposite side due to periodic boundary conditions. Both walls consist of two layers of argon atoms (each layer containing 128 atoms) fixed in a face centered cubic (fcc) lattice (100 direction). The fluid-wall interaction is equal to the fluid-fluid interaction and the reduced density of the system is $\rho^* = 0.8$ (corresponding to a volume fraction of $\nu = 0.415$). Physical quantities are nondimensionalized by using the length, energy and mass scales of liquid argon, which are $\sigma = 3.405 \times 10^{-10}$ m, $\epsilon = 1.67 \times 10^{-21}$ J and $m = 6.626 \times 10^{-26}$ kg respectively. A constant body force f^* acts on the fluid in negative z-direction, causing it to flow. The mutual interaction of the neutral spherically symmetric argon atoms is modeled via a two-body Lennard-Jones (LJ) potential:

$$U(r) = 4\epsilon \left(\left(\frac{\sigma}{r} \right)^{12} - \left(\frac{\sigma}{r} \right)^{6} \right), \qquad (1)$$

with r the distance between two atom centers. From the interaction potential, the force between two atoms can be calculated:

$$F_{LJ}(r) = -\frac{\partial U}{\partial r} = 24\frac{\epsilon}{\sigma} \left(2\left(\frac{\sigma}{r} \right)^{13} - \left(\frac{\sigma}{r} \right)^{7} \right). \quad (2)$$

The force is truncated at $r_c = 2.5\sigma$ in order to reduce calculation time, therefore $F(r \geq r_c) = 0$. Furthermore, the force is shifted with $F(r_c)$ in order to maintain a continuous force at the location of truncation:

$$F(r) = 24\frac{\epsilon}{\sigma} \left(2\left(\frac{\sigma}{r} \right)^{13} - \left(\frac{\sigma}{r} \right)^{7} \right) - F_{LJ}(r_c). \quad (3)$$

The natural time step, $\tau = (m\sigma^2/\epsilon)^{1/2}$, is proportional to the period of oscillation around the potential minimum. For liquid argon, it is $\tau = 2.14 \times 10^{-12}$ s. From the positions, velocities and interatomic forces, other physical scalar or tensorial quantities can be calculated (e.g. shear rate, stress and viscosity) [Hartkamp

et al. (2010)]. The position and momentum of every atom and the forces acting on them are used to calculate their position and velocity after an increment (Δt) in time via the Velocity Verlet algorithm, with a time step of $t = 0.001\tau$. The body force leads to an acceleration of the fluid, while viscous effects retard the flow until a steady state is reached. Local thermostats near the walls keep the energy (and thus the temperature) constant in time ($T^* = 1.0$ for the simulations presented here) [Ghosh *et al.* (2007); Bartos & Jánosi (2007)]. Atoms are initially positioned on an fcc lattice. The lattice melts during the equilibration, followed by a steady state simulation. The steady-state simulation results are averaged over a period of time of the order of $1000\tau - 5000\tau$. Furthermore, spatial averaging is employed over the directions parallel to the solid walls, whereas, the x-direction (perpendicular to the solid walls) is divided into equally spaced bins of width $b = 0.083$.

In the following sections we first discuss the density profile and its relation to the channel width. Next, the computation of the local stresses in the fluid is discussed. Some results are presented for the stresses across the channel. Finally, the presented theory and results are discussed and certain topics and ideas for future work are briefly motivated.

Density

Fig. 2 shows a volume fraction profile in the channel for different channel widths. Each of the profiles shows oscillatory behavior near the channel walls which decays exponentially away from the walls. The peak closest to the wall is due to the wall atoms, the density of the fluid goes to zero there. The period and magnitude of the most apparent oscillations in the fluid density seems to be approximately identical for all three simulations (apart from statistical noise). The oscillatory density profile near the wall can be captured by a function of

2

the following form:

$$\nu(x) = \nu_0 + \alpha \cos\left(\pm \frac{2\pi}{L}(x - x_w)\right)\exp\left(\frac{\mp(x - x_w)}{x_0}\right).$$
(4)

The $\pm$ and $\mp$ signs correspond to a fit near the left and the right wall respectively. Physical properties, such as the bulk volume fraction ν_0 and the period ($\sim$ wavelength) L of the density oscillations, can be identified. The exponential decay away from the wall is quantified by x_0 and the amplitude of the density oscillations (at the wall) are fitted with α. It must be noted that, unlike the period of oscillation and the bulk volume fraction, the amplitude and decay of the oscillatory peaks, are strongly dependent on the coarse graining of the data (in this work, a Gaussian function is used to coarsegrain the information). A least-squares fit of the data is made, where the oscillation closest to the wall is not taken into account since this data does not solely represent the density of the fluid, but also the wall particles are contributing. Table 1 shows the parameter values for a least-squares fit of the left and right half of the channel of width $W_3 = 16.245\sigma$ and Fig. 3 shows the simulation data and the exponential fit. The value for L shows that the approximate period of the oscillations is smaller than the length scale of the argon atoms for this simulation, but larger than the initial lattice spacing, which is 0.855σ. The period of the oscillations, however, does depend on the average density and temperature in the system (data not shown). The bulk volume fraction ν_0 is (almost) equal to the average volume fraction in the system, these values could deviate for example in a simulation where the parameters for interaction between the fluid and the wall are different from the interaction between fluid particles.

Table 1: Fitting parameters.

Parameter	Left	Right
ν_0	0.4146	0.4146
α	0.2324	0.2322
x_w	0.0	16.245
L	0.9326	0.9322
x_0	1.1509	1.2010

In the largest system shown in Fig. 2, a bulk fluid-like (i.e. homogeneous) region can be identified in the center. Six distinct peaks are observed between each wall and the bulk fluid region of the channel. Decreasing the system size, but keeping the density and temperature unchanged, the homogeneous region shrinks in size and finally disappears when the channel width becomes smaller than approximately 12σ. For narrower channels, a region forms in the center where the oscillations in

(a)

(b)
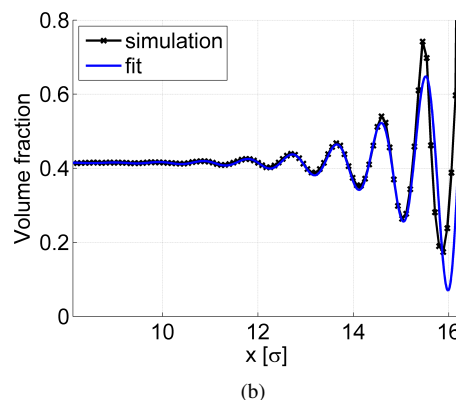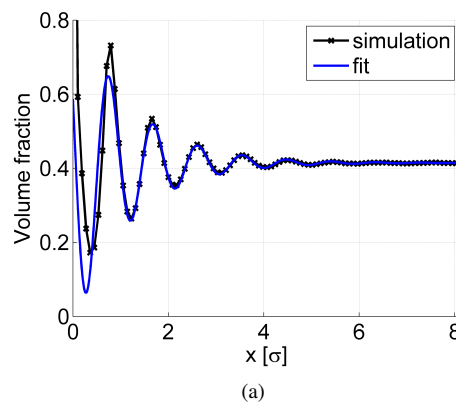
Figure 3: (a) Volume fraction in the left half of the channel. (b) Volume fraction in the right half of the channel.

density, induced by both walls, interfere additively; the oscillatory behavior in this region becomes directly dependent on the system size. It will be shown that by simply taking the density profile in the left and right inhomogeneous region of the largest system, one can predict the density profile in a system that is either larger or smaller. Consider the density profile in the left and right half of a channel that is wider than twice the inhomogeneous region (a channel of width $W_3 = 16.245\sigma$ is used here) and shift these towards each other until a channel of width $W_2 = 11.115\sigma$ is realized. The deviations from the average density are then just summed up. In Fig. 4, the constructed profile is compared to the result of a molecular dynamics simulation.

The figure confirms that the interference of the oscillations is only significant in the region that is within 6σ distance from both walls and that the oscillations can be summed up approximately. The region where the influence of both walls overlaps is small in this system (W_2) and so is the amplitude of the oscillations. If we apply the same approach to a more narrow channel (W_1)(see Fig. 5), where the overlapping region dominates the sys-

(a)

(b)
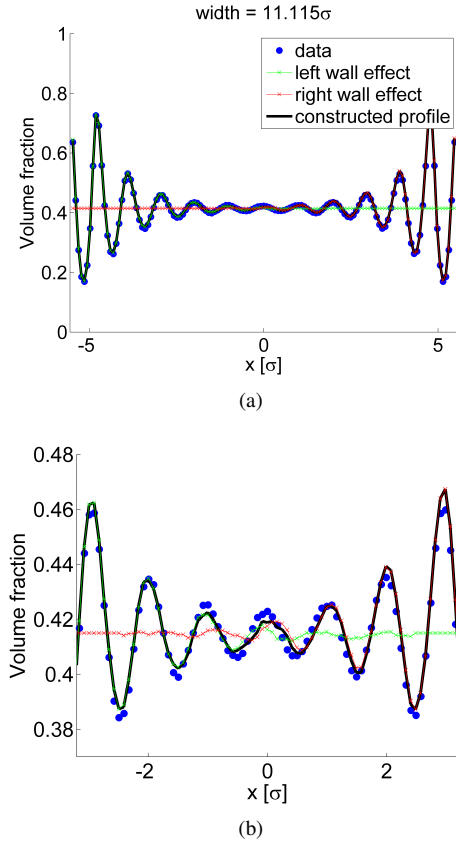
Figure 4: (a) Comparison of a constructed density profile and the data of a molecular dynamics simulation for a channel of width $W_2 = 11.115\sigma$. (b) Close-up of the center of the channel in (a).

tem (i.e. the density profile in the whole system is directly influenced by both walls), we see a great correspondence to the density profile that was obtained by a molecular dynamics simulation, in both the magnitude and period of the oscillations.

The approach that was presented here can be used to predict the oscillatory behavior in a channel without having to simulate the system explicitly. However, more extensive testing of the method is required, especially when the system width decreases below 5.985σ and for systems with other densities and temperatures. If a quantitative relation between the density profile and other physical properties can be found for this inhomogeneous channel flow, the method presented here could predict layering and the flow behavior of the fluid without the need of simulating every individual system width explicitly.
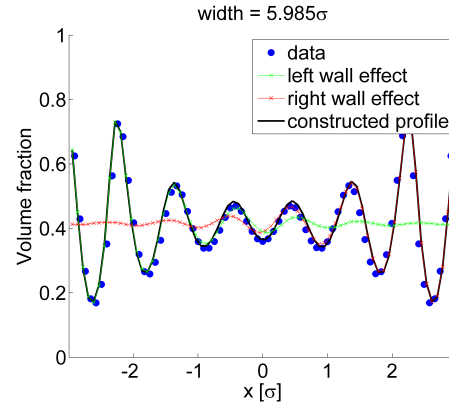
Figure 5: The comparison of a constructed density profile and the data of a molecular dynamics simulation for a channel of width $W_1 = 5.985\sigma$.

Stress

Molecular dynamics simulations evolved over the last decades to a much used tool for studying many types of small-scale problems. Yet, how to calculate the macroscopic stress from microscopic information of individual particles and interactions is still a much debated subject. An important similarity between continuum mechanics and molecular dynamics is that they both have to obey the conservation of mass and momentum.

The virial stress is often used to calculate the stresses in atomic systems. The virial stress expression was first derived by Lutsko (1988), based on a generalization of the virial theorem presented by Clausius (1870). No formulation of the virial stress is fully accepted to date. Zhou (2003) wrongly argues that the virial stress is totally irrelevant to the mechanical stress and has no physical significance at all. One of the arguments that Zhou presents is that momentum can only be transported by mass, and force can only work on a mass. This belief is contradictory to the generalization made by Lutsko, according to Zhou. In response, a number of articles were published, showing the physical significance of the virial stress (van Dommelen (2003); Subramaniyan & Sun (2008)). The formulation used here is in accordance with Todd *et al.* (1995), apart from details discussed below.

The virial stress is given as the sum of a kinetic part, which accounts for the momentum transport of the particles, and a potential part, which represents the contribution of the interaction between all pairs of particles:

$$\Pi_{ij}^{bin}(x) = \Pi_{ij}^{k}(x) + \Pi_{ij}^{u}(x). \tag{5}$$

The sum of the kinetic and potential contribution is sometimes multiplied with a Dirac delta function (Eq. 1.7 in Zhou (2003)), which assigns a location to the

atomic stress contribution. While this approach is simple and mathematically convenient, we believe that the kinetic and the potential term should be coarse-grained individually as shown below.

The kinetic stress contribution in a bin yields:

$$\Pi_{ij}^k(x) = \frac{1}{V_{bin}} \sum_{p \in bin} m^p \tilde{v}_i^p \tilde{v}_j^p \Phi^p(x), \qquad (6)$$

where m^p is the mass of the particles, $\Phi^p(x)$ represents a coarse graining function and $\tilde{v}_i^p = (v_i^p - u_i(x^p))$ is the fluctuation velocity of a particle p (i.e. the difference between the particle velocity and the local streaming velocity), where $u_i(x^p)$ is the local streaming velocity (subscript i indicates the components in the i-direction), defined here as the average velocity of particles in the bin averaged over time. This approach results in a streaming velocity which slightly depends on the spatial discretization. This dependence disappears in the limit of small bins and large averaging time, however, a proper smoothing of the data is paramount. The fluctuation velocity is generally used for the calculation of kinetic properties such as temperature or the kinetic part of stress. Some authors have used the total velocity of the particle rather than the fluctuation velocity, however, stress obtained with total velocities is not objective.

The potential energy contribution of stress is obtained by computing the change in the potential energy density (due to a virtual deformation) with respect to the components of the deformation tensor (ϵ_{ij}):

$$\Pi_{ij}^u(x) = \frac{\partial U}{\partial \epsilon_{ij}}. \qquad (7)$$

Following the above expression, through some calculations it can be shown that the potential stress tensor can be obtained from the pairwise interactions as:

$$\Pi_{ij}^u(x) = \frac{1}{2V_{bin}} \sum_{p \in bin} \sum_{q \neq p}^N r_i^{pq} F_j^{pq} \Phi^{pq}(x), \qquad (8)$$

where compressive stresses are defined to be positive here. The so-called branch vector component $r_i^{pq} = r_i^p - r_i^q$ denotes the ith component of the distance vector between particles p and q and F_j^{pq} the jth component of the interaction force between particles p and q as defined in Eq. (3).

The potential stress contribution contains a coarse graining function, $\Phi^{pq}(x)$, in which the distribution of information over the branch vector between the particles is modeled. The formulation presented here does not impose restrictions on the coarse-graining functions (for either part of the stress tensor). A more extensive discussion about these functions is given in Hartkamp et al. (2010).
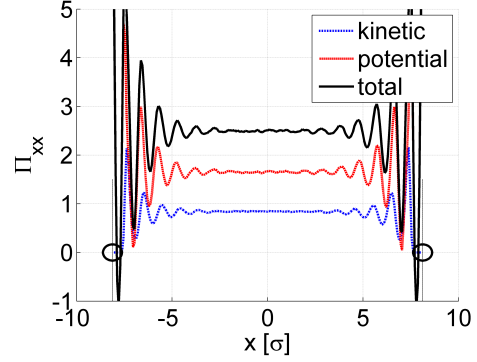
Figure 6: The kinetic and potential contributions to the stress term Π_{xx} across the channel.

The factor $1/2$ in Eq. (8) accounts for the fact that in this expression each pair interaction is taken into account twice. Since Newton's third law states that: $F_j^{pq} = -F_j^{qp}$, Eq. (8) can be reduced to:

$$\Pi_{ij}^u(x) = \frac{1}{V_{bin}} \sum_{p \in bin} \sum_{q > p}^N r_i^{pq} F_j^{pq} \Phi^{pq}(x). \qquad (9)$$

The presented expression for $\Pi_{ij}^k(x)$ and $\Pi_{ij}^u(x)$ are instantaneous atomic stress contributions. These instantaneous quantities have rather strong fluctuations, however, averaging both terms over time results in the continuum Cauchy stress (Subramaniyan & Sun (2008)).

Results

The stresses in the system of 16.245σ width, a reduced density of $\rho^* = 0.8$ and a reduced body force of $f^* = 0.1$ are presented here. Figs. 6, 7, and 8 show the normal stresses in the x, y and z-direction respectively. In the bulk, the normal stresses are approximately equal in each direction. Near the wall, oscillations occur, similar to the oscillations in density shown above. The oscillations are not identical for the different normal directions, indicating anisotropy in this region. The normal stress Π_{xx} in the direction of confinement (i.e. perpendicular to the walls) shows larger oscillations in comparison to the directions parallel to the walls. The negative values for stress correspond to tensile stresses, these can occur locally in an anisotropic fluid, however, more study is required in order to fully understand this local stress behavior and the influence of the coarse graining procedure on it. The hydrostatic pressure (Fig. 9) follows from the average of the normal stresses $p = (\Pi_{xx} + \Pi_{yy} + \Pi_{zz})/3$.

Fig. 10 shows the shear stress Π_{xz} across the channel. The kinetic contribution is very small compared to the potential part of the shear stress. The shear stress
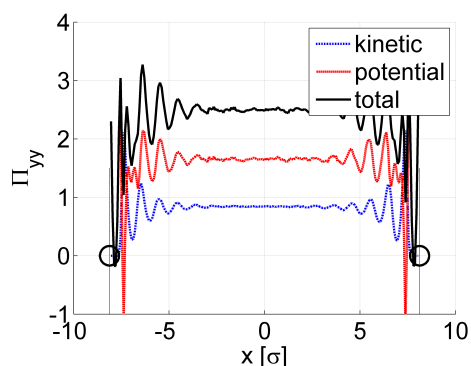
Figure 7: The kinetic and potential contributions to the stress term Π_{yy} across the channel.
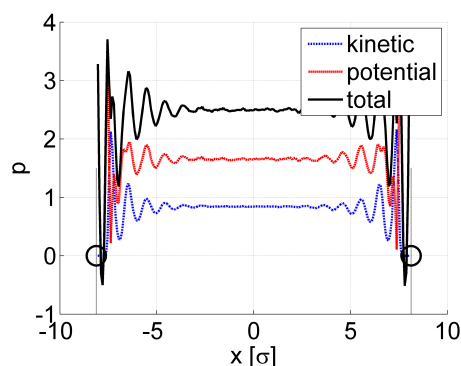
Figure 9: The kinetic and potential contributions to the hydrostatic pressure across the channel.
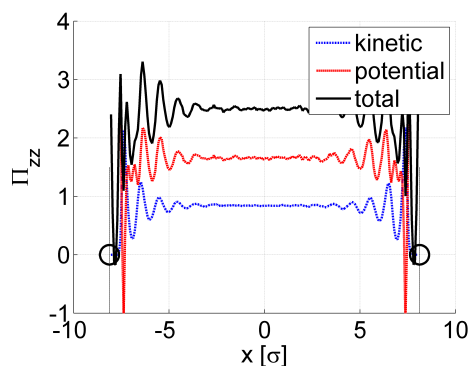
Figure 8: The kinetic and potential contributions to the stress term Π_{zz} across the channel.
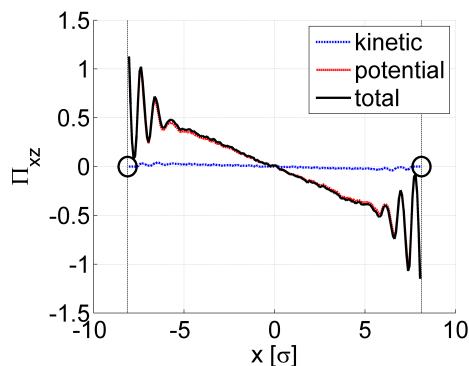
Figure 10: The kinetic and potential contributions to the stress term Π_{xz} across the channel.

shows oscillations superimposed on a linear trend across the channel. The linear trend corresponds to the shear stress in a Newtonian fluid, whereas, the oscillations again represent the deviations from a Newtonian fluid. The kinetic and potential contribution of the other non-diagonal components of the stress tensor, Π_{xy} and Π_{yz}, are fluctuating around zero, as may be expected.

Discussion and future work

Molecular dynamics simulations are performed for a noble fluid in a nanochannel. It is shown here, that the oscillations in density, close to the wall, can be characterized by a certain period L, amplitude α and decay length x_0. A likely dependence on average density, temperature and interaction parameters is not studied here.

The calculation of stress in a nanochannel is discussed. Analyzing the local stresses in a strongly confined fluid system is important in order to study properties such as anisotropy. Due to the inhomogeneity in these systems, the flow behavior deviates from that of a Newtonian fluid. A better understanding of oscillatory behavior in the density and stress terms is paramount to deriving a new constitutive model that captures the non-Newtonian behavior of the fluid. In addition to the total virial stress, results are shown for the kinetic and potential contribution to the virial stress. The results show that, while the potential part dominates over the kinetic part, neither contribution is negligibly small for the normal stresses in the present situation. Only the kinetic contribution to Π_{xz} is very small compared to the potential contribution.

The local value of various physical quantities depend on a the spatial discretization and a proper coarse graining of the information, as mentioned above. The width of the bins determines the resolution of the averaged data. Decreasing the bin size, results in fewer atoms per bin, and thus worse statistics. The quality of the statistics can be improved by coarse graining of the data with some type of non-local smoothing function. The physical justification for this action is the fact that particles have a finite size. Since atoms don't have a specified exact radius, a Gaussian distribution is suitable to distribute the information of an atom over space (e.g.

for Φ^p in Eq. (6)). Similarly, the force between an interacting particle pair does not act solely on the center of the atom. Thus, also a coarse graining function is needed to describe the microscopic force field (Φ^{pq} in Eq. (9)), since atoms do not have a force concentration on a well-defined contact point, such as interacting macroscopic particles have. Little is known about how to distribute the information of an atomic (long-range) interaction over space. Goldhirsch (2010) developed a promising method to coarse-grain microscopic information of interacting particles. A more elaborate analysis of this method will be given in later work.

The results from the virial stress can be verified by calculating the force (rate of change in momentum) on the walls of a simulation system. Dividing this force by the area of the walls gives the corresponding stress vector and stress components. The obtained values can be compared to those obtained from the virial stress. This method is pretty straightforward for a system in which the particles have no average streaming velocity (i.e. no body force acts on the particles).

Acknowledgements

References

Bartos I. and Jánosi I.M., Side pressure anomalies in 2D packings of frictionless spheres, Granular Matter, Vol. 9, pp. 81, 2007

van den Berg A., Sparreboom W. and Eijkel J.C.T., Principles and applications of nanofluidic transport, Nature Nanotechnology, Vol. 4, pp. 713, 2009

Bitsanis I., Vanderlick T.K., Tirrell M. and Davis H.T., A tractable molecular theory of flow in strongly inhomogeneous fluids, Journal of Chemical Physics, Vol. 89, pp. 3152, 1988

Clausius R., On a mechanical theory applicable to heat., Philosophical Magazine, Vol. 40, pp. 122-127, 1870

van Dommelen L., Physical interpretation of the virial stress, http://www.eng.fsu.edu/ dommelen/papers/virial/index.pdf, 2003

Ghosh A., Paredes R. and Luding S., Poiseuille flow in a nanochannel - use of different thermostats, International Congress of Particle Technology, CD Proceedings, pp. 1-4, 2007

Goldhirsch I., Stress, stress asymmetry and couple stress: from discrete particles to continuous fields, Granular Matter, Vol. 12, in press, 2010

van Gunsteren W.F., Berendsen H.J.C., Postma J.P.M., DiNola A. and Haak J.R., Molecular Dynamics with Coupling to an external bath, Journal of Chemical Physics, Vol. 81, pp. 3684, 1984

Hartkamp R.M., Ghosh A. and Luding S., Anisotropy of a fluid confined in a nanochannel, In preparation, 2010

Koplik J. and Banavar J.R., Molecular dynamics simulation of microscale poiseuille flow and moving contact lines, Physical Review Letters, Vol. 60, pp. 1282, 1988

Lutsko J.F., Stress and elastic constants in anisotropic solids: Molecular dynamics techniques, Journal of Applied Physics, Vol. 64, pp. 1152, 1988

Subramaniyan A.K. and Sun C.T., Continuum interpretation of virial stress in molecular simulations, International Journal of Solids and Structures, Vol. 45, pp. 4340-4346, 2008

Todd B.D. and Evans D.J., The heat flux vector for highly inhomogeneous non-equilibrium fluids in very narrow pores, Journal of Chemical Physics, Vol. 103, pp. 9804, 1995

Todd B.D., Evans D.J. and Daivis, P.J., Pressure tensor for inhomogeneous fluids, Phys. Rev. E, Vol. 52, pp. 1627, 1995

Travis K.P., Todd B.D. and Evans D.J., Departure from Navier-Stokes hydrodynamics in confined liquids, Physical Review E, Vol. 55, pp. 4288, 1997

Travis K.P. and Gubbins K.E., Poiseuille flow of Lennard-Jones fluids in narrow slit pores, Journal of Chemical Physics, Vol. 112, pp. 1984, 2000

Zhou M., A new look at the atomic level virial stress: on continuum-molecular system equivalence, Proceedings of the Royal Society of London. Series A: Mathematical, Physical and Engineering Sciences, Vol. 459, pp. 2347-2392, 2003